Geophysical observations of Phobos transits by InSight

Simon C. Stähler[1], Rudolf Widmer-Schnidrig[2], John-Robert Scholz[3], Martin van Driel[4], Anna Magdalena Mittelholz[5], Kenneth Hurst[6], Catherine L. Johnson[7], Mark T Lemmon[8], Ralph D. Lorenz[9], Philippe Henri Lognonné[10], Nils T Mueller[11], Laurent Pou[12], Aymeric Spiga[13], Donald Banfield[14], Savas Ceylan[15], Constantinos Charalambous[16], Domenico Giardini[4], Francis Nimmo[17], Mark Paul Panning[18], Walter Zürn[19], and William Bruce Banerdt[20]

[1]Eidgenössische Technische Hochschule Zürich
[2]Black Forest Observatory, Institute of Geodesy, Stuttgart University, Heubach 206, D-77709 Wolfach, Germany
[3]Max Planck Institute for Solar System Research, Justus-von-Liebig-Weg 3, 37077 Göttingen, Germany
[4]ETH Zürich
[5]The University of British Columbia
[6]Jet Propulsion Laboratory, California Institute of Technology, Pasadena, CA 91109, USA
[7]University of British Columbia
[8]Space Science Institute
[9]Johns Hopkins University Applied Physics Lab
[10]Institut de Physique du Globe de Paris et Université de Paris Diderot
[11]German Aerospace Center (DLR), Institute of Planetary Research
[12]Dept. of Earth and Planetary Sciences, University of California Santa Cruz, Santa Cruz, CA 95064, USA
[13]Sorbonne Université (Faculté des Sciences)
[14]Cornell
[15]ETH Zurich
[16]Imperial College London
[17]University of California, Santa Cruz
[18]Jet Propulsion Laboratory, California Institute of Technology
[19]Black Forest Observatory (Schiltach), Universities Karlsruhe/Stuttgart
[20]Jet Propulsion Laboratory

November 21, 2022

Abstract

Since landing on Mars, the NASA InSight lander has witnessed 8 Phobos and one Deimos transit. All transits could be observed by a drop in the solar array current and the surface temperature, but more surprisingly, for several ones, a clear signature was recorded with the seismic sensors and the magnetometer. We present a preliminary interpretation of the seismometer data as temperature induced local deformation of the ground, supported by terrestrial analog experiments and finite-element modelling. The magnetic signature is most likely induced by changing currents from the solar arrays. While the observations are not fully

understood yet, the recording of transit-related phenomena with high sampling rate will allow more precise measurements of the transit times, thus providing additional constraints for the orbital parameters of Phobos. The response of the seismometer can potentially also be used to constrain the thermo-elastic properties of the shallow regolith at the landing site.

Geophysical observations of Phobos transits by InSight

S. C. Stähler[1], R. Widmer-Schnidrig[2], J.-R. Scholz[3], M. van Driel[1], A. Mittelholz[4], K. Hurst[5], C. L. Johnson[5,6], M. T. Lemmon[7], R. D. Lorenz[8], P. Lognonné[9], N. T. Müller[10], L. Pou[11], A. Spiga[12,13], D. Banfield[14], S. Ceylan[1], C. Charalambous[15], D. Giardini[1], F. Nimmo[11], M. Panning[5], W. Zürn[16], W. B. Banerdt[5]

[1]Institute of Geophysics, ETH Zürich, Sonneggstrasse 5, 8092 Zürich, Switzerland
[2]Black Forest Observatory, Institute of Geodesy, Stuttgart University, Heubach 206, D-77709 Wolfach, Germany
[3]Max Planck Institute for Solar System Research, Justus-von-Liebig-Weg 3, 37077 Göttingen, Germany
[4]Department of Earth, Ocean and Atmospheric Sciences, University of British Columbia, Vancouver, BC, V6T 1Z4, Canada
[5]Jet Propulsion Laboratory, California Institute of Technology, Pasadena, CA 91109, USA
[6]Planetary Science Institute, Tucson, AZ 85719, USA
[7]Space Science Institute, Boulder, CO, USA
[8]Johns Hopkins Applied Physics Laboratory, 11100 Johns Hopkins Road, Laurel, MD 20723, USA
[9]Université de Paris, Institut de physique du globe de Paris, CNRS, F-75005 Paris, France
[10]German Aerospace Center (DLR), Institute of Planetary Research, Rutherfordstr. 2, 12489 Berlin, Germany
[11]Dept. of Earth and Planetary Sciences, University of California Santa Cruz, Santa Cruz, CA 95064, USA
[12]Laboratoire de Météorologie Dynamique / Institut Pierre Simon Laplace (LMD/IPSL), Sorbonne Université, Centre National de la Recherche Scientifique (CNRS), École Polytechnique, École Normale Supérieure (ENS), Campus Pierre et Marie Curie BC99, 4 place Jussieu, 75005 Paris, France
[13]Institut Universitaire de France, 1 rue Descartes, 75005 Paris, France
[14]Cornell University, Cornell Center for Astrophysics and Planetary Science, Ithaca, NY, 14853, USA
[15]Department of Electrical and Electronic Engineering, Imperial College London, London, UK
[16]Black Forest Observatory, KIT Karlsruhe, Heubach 206, D-77709 Wolfach, Germany

Key Points:

- Multiple geophysical instruments on InSight observe unexpected signals during Phobos transits.
- Local ground deformation due to insolation change can explain the seismometer signal.
- The dropping solar array currents result in a change in the magnetic field.

Corresponding author: S. C. Stähler, `simon.staehler@erdw.ethz.ch`

Abstract

Since landing on Mars, the NASA InSight lander has witnessed 8 Phobos and one Deimos transit. All transits could be observed by a drop in the solar array current and the surface temperature, but more surprisingly, for several ones, a clear signature was recorded with the seismic sensors and the magnetometer. We present a preliminary interpretation of the seismometer data as temperature induced local deformation of the ground, supported by terrestrial analog experiments and finite-element modelling. The magnetic signature is most likely induced by changing currents from the solar arrays. While the observations are not fully understood yet, the recording of transit-related phenomena with high sampling rate will allow more precise measurements of the transit times, thus providing additional constraints for the orbital parameters of Phobos. The response of the seismometer can potentially also be used to constrain the thermo-elastic properties of the shallow regolith at the landing site.

Plain Language Summary

The geophysical lander station, InSight, has been operating on the surface of Mars since November 2018. Since then, the martian moons Phobos and Deimos have been partially blocking the sun, as seen from the InSight landing site, multiple times. Multiple InSight instruments have been measuring the effect of those transits; this surprisingly includes the seismometer and the magnetometer. We conclude that temperature induced deformation and tilt is responsible for the the seismic measurements. The magnetometer measurements are most likely result of a drop in the solar array currents. We do not observe atmospheric modulations with InSight's weather station during the transit. These observations help constrain orbital parameters of the martian moons and the seismometer signal might allow investigating thermo-elastic properties of the shallow martian material.

1 Introduction

The small martian satellites Phobos and Deimos orbit in synchronous rotation with inclinations of less than one degree (Grier & Rivkin, 2019). For observers, or robot landers at near-equatorial latitudes it is therefore possible to observe solar transits by both satellites (Ledger, 1879), in blocks of up to five transits, twice per Martian year. The first observation of an transit from the surface of Mars was done by using the scan camera on the Viking 1 lander as a brightness detector (Duxbury, 1978; Christou, 2002). The first actual image of Phobos and Deimos transiting the Sun was captured by the Spirit and Opportunity rovers (Mars Exploration Rovers A and B) in 2004 (Bell et al., 2005). The determination of transit timing allows to update ephemeris tables, which are crucial for missions targeting the moons (Usui et al., 2018). They also determine the moons' secular acceleration, from which the tidal dissipation in the Martian mantle can be estimated (Bills et al., 2005; Nimmo & Faul, 2013; Khan et al., 2018). Further observations of Phobos transits from fixed reference positions on the surface are therefore highly desired.

Here we discuss the main Phobos and Deimos transits experienced by the InSight lander in the first 500 sols since its arrival at the surface of Mars on November 26th 2018. InSight features a fully-deployed shielded seismometer on the surface of Mars, as well as sensors probing the atmospheric, magnetic and surface environments. Furthermore, of interest for transit studies, the InSight lander has been located independently from orbital imaging and the radio tracking experiment RISE onboard (Folkner et al., 2018) and can be considered the best-constrained location on the planet at 4.50238417°N, 135.62344690°E, at an elevation of -2613.426 m with respect to the MOLA geoid (Golombek et al., n.d., ground under spacecraft deck center, see).

Rapid change in irradiation by moving cloud shadows is known to correlate with tilt-like signals on surface-installed seismometers. While no literature on the topic seems to exist, it has been described by operators of temporary networks that despite extensive thermal shielding (Karin Sigloch, personal communication, 2012). Schweitzer et al. (2014) mitigated horizontal low-frequency noise at the Antarctic station TROLL by covering the granite surface surrounding the seismometer with loose rocks to shield the bed rock from direct sun light, using insights from experiments with transient heat sources on a well shielded vault seismometer (Zürn & Otto (2000)). While not changing the thermal isolation of the seismometer, these measures had a large impact on low-frequency noise levels.

Earth observations have shown that solar eclipses can lead to changes in ionospheric currents, due to a drop in electron density of 35% (Reinisch et al., 2018; Huba & Drob, 2017). On Earth the effect on the geomagnetic field varies depending on the solar conditions and activity level in the external fields, and is often too subtle to be detected on an individual eclipse requiring statistical analyses of many events (Kim & Chang, 2018).

We first discuss the observations of the individual instruments and present a common explanation framework afterwards.

2 Observations

2.1 Observations with Solar Arrays

The most immediate surface manifestation of an eclipse or a transit on Earth or Mars is the drop in sunlight due to the geometric obstruction of part of the solar disk. For Phobos, this can reach around 40%. The current generated by the InSight solar arrays is monitored when the lander is awake and is recorded with a precision of about 0.1% (for noon sunlight levels) at a sample interval of around 30s until September 2019 and 4s afterwards (Lorenz, Lemmon, Maki, et al., 2020).

A 120-s transit of Deimos with a transit depth of 1% was observed on Sol 481 (Lorenz, Lemmon, & Mueller, 2020). Phobos transit depths are usually deeper but briefer, the drop in solar array currents are lower than the predicted geometric obstructions. Observed depths on Sols 495, 498, 499 and 501 were 4, 12, 10 and 23% respectively, these being 0.5, 0.7, 0.7 and 0.85 of the predictions (see also table 1). The difference is assumed to reflect the contribution of light scattered by dust in the sky outside of the Phobos shadow, which makes a more significant relative contribution when the Sun is low. Since scattered light affects the surface heat budget in the same way as direct sunlight, the solar array current is then a useful measure of the total solar forcing for modeling any thermal effects.

The Sol 96-99 Phobos transits of spring 2019 were detected as single-sample current drops, confirming their occurrence, but precluding quantitative analysis (Lorenz, Lemmon, Maki, et al., 2020).

2.2 Observations with the seismometer

Three of the six Phobos transits that occurred between InSight landing and today (see Tab. 1, not counting grazing transits) produced some observable signal on SEIS' very broadband seismometer (VBB) and short period seismometer (SP) (green = clear signal above noise level; orange = increased noise level but signal still observable; red = no clear signal). After correction for instrument response, these three transits all have a clear signal with an acceleration amplitude of ~ 50 nms^{-2} and a duration of ~ 100 s. Rotation into a ZNE coordinate system shows a first pulse of positive polarity on both horizontal components with a duration of 30 seconds, followed by a decaying part of about 70 seconds. There is no clear signal on the vertical component for any transit event.

All three transits seen by VBB and SP occur around midday local true solar time (LTST) when the Sun is high in the sky whilst all other eclipses not observed by VBB and SP do not occur around noon LTST. For these, the corresponding tilt azimuths (determined via linear polarization analysis) point away from the connector of the tether connecting SEIS to the lander, which is located at an azimuth $\sim 15°$. Tilt angles θ were derived from the peak-to-peak amplitude of filtered radial acceleration data during the transit (a_R), following $\sin(\theta) \approx \theta = a_R/g_{\mathrm{Mars}}$, with $g_{\mathrm{Mars}} = 3.71 \mathrm{ms}^{-2}$. Acceleration and tilt errors, estimated via the data standard deviation using a 300 s window before and after the transit, are about 10%. The Deimos transit does not produce a clear signal on SEIS (Tab. 1). A measurement example for the Phobos transit on Sol 501 is given in the electronic supplements Fig. SI-2.

The onset of the VBB signal is delayed by 5 s, relative to the first contact of Phobos with the sun and also with respect to the solar array current and the magnetometer channels (see below).

2.3 Observations with the magnetometer

We assess the magnetic field signals associated with all listed transits (table 1). For the earlier transits (up to sol 99) the InSight fluxgate magnetometer (IFG) data are sampled at 0.2 Hz; for the

later transits, the data rates are increased to 2 Hz. Magnetic field perturbations are seen associated with Phobos transits on sols 96, 97 and 501 (supp. figure 1), with different relative contributions from each component for individual transits. All other transits did not result in a detectable magnetic field signal (table 1).

We investigated possible mechanisms that could cause the observed response, focusing on three aspects: (1) The IFG response to temperature and solar array current fluctuations, (2) tilt as a result of differential contraction of the lander legs, and (3) an ionospheric response.

2.3.1 *Temperature and Solar Array Current*

The IFG is affected by changes in temperature and solar array currents. The data processing pipeline attempts to correct for these effects, in particular on diurnal time scales. However, the lack of a pre-launch magnetic cleanliness program or comprehensive calibrations, means that small residual effects may still be present (Joy et al., 2019). The IFG electronics and sensor temperatures, showed no signals related to the transits and we excluded those as possible reasons for the observed IFG response. However, the decrease in incoming sunlight resulted in changes in the solar array currents (Table 1). Transits that resulted in measurable magnetic fields responses are all associated with current drops larger than 0.01 A on channels E-0771 and E-0991. The effect of solar array currents on the IFG data was not tested pre-flight, however, an order of magnitude calculation assuming a line current approximately 1 m from the IFG instrument, indicates that a 3 nT change in the IFG data would require a $\sim$0.015 A drop in the current which is approximately consistent with observations.

2.3.2 *Tilt*

Differential thermal contraction of the three lander legs could lead to tilt of the lander deck and the IFG. At local noon two legs are in full sun light while the third leg on the North side of the lander is partially shaded by the deck leading to the deck tilting south during the Phobos transit. However a tilt of the magnetometer would not affect the magnitude of the overall signal but only the individual components. The IFG data during transits with a detectable signal do not support the tilt hypothesis as the magnitude $|B|$ drops by up to 2.1 nT during the transit (Table 1).

2.3.3 *Ionosphere*

The magnetic field can result from electric currents in the ionosphere, driven by atmospheric winds between $\sim$130 km and $\sim$180 km altitude. A drop in electron density associated with an eclipse might lead to changes in ionospheric currents. Drops up to 35% in electron density have been observed for Solar eclipses on Earth (Reinisch et al., 2018; Huba & Drob, 2017), but such eclipses last much longer ($\sim$3 hours) than the transits discussed here. Thus, ionospheric effects are expected to be correspondingly smaller on Mars.

Although the magnetic field associated with the drops could be affected by changes in ionospheric currents, the signals that were recorded would require large, instantaneous responses, temporally correlated only with the Phobos shadow passing over the InSight landing site, which is unphysical. Also, during a near-miss transit, no signal could be detected.

2.4 Observations with InSight's weather station

The InSight lander is equipped with a weather station capable to assess atmospheric conditions for seismic observations (Banfield et al., 2018; Spiga et al., 2018). We assess the pressure, temperature and wind signal associated with the 3 Phobos transits for which we observe both seismic and magnetic signals. For the earlier transits (up to sol 99) pressure / wind-temperature measurements are available sampled at 0.1 / 2 Hz; for the later transits, the data rates are increased to 1 / 10 Hz.

No particular distinctive signatures associated with the transits can be found in the atmospheric observations – even in the case of the major Phobos transit on sol 501. The fluctuations of pressure, wind, and temperature during the transit are governed by the characteristic convective turbulence on Mars in the daytime hours (Banfield et al., 2020).

In the daytime hours prone to strong turbulence on Mars, two distinctive atmosphere-induced seismic signatures are found: broad-band noise from wind and transient signatures associated with dust-devil-like convective vortices Garcia et al. (2020); Murdoch et al. (under review in this issue); Kenda et al. (2020) We performed a vortex search following the approach detailed in Banfield et al. (2020) and Spiga et al. (submitted to this issue). No convective vortex was detected during either the major sol 501 Phobos transit or the sols 96-97 transits, ruling out this seismic source. The sol 501 Phobos transit actually occurred at a season when the vortex encounters at the InSight landing site have significantly declined. Furthermore, Wind noise due to turbulence during the three transits is uneventful, behaving like turbulent noise in normal conditions.

2.5 Radiometer Observations

The Heatflow and Physical Properties Package (HP^3) includes an infrared radiometer to monitor surface temperature in two spots approximately 1.5 and 3 m to the NNW of the lander deck center (Spohn et al., 2018). For an interval 20 min around the transits on sol 96, 97, 99, 497, 498 and 501, the radiometer observed with its maximum sampling rate of 0.46 Hz. The 1σ instrumental noise of the instrument is equivalent to a temperature difference of less than 0.25 K during the time of the transits (N. Mueller et al., 2020), and the temperature response to the transits is clearly visible (Fig. 1). The temperature response is larger than we expected based on preliminary calculations using the surface thermal inertia of 190 ± 30 $\text{Jm}^{-2}\text{K}^{-1}\text{s}^{-1/2}$ derived from the the diurnal temperature curve (Golombek et al., 2020). This is similar to the remote observation of the temperature response to the transit by the Soviet Phobos '88 spacecraft, which was larger than expected based on the diurnal temperature response (Betts et al., 1995). This is consistent with less dense and/or lower thermal condictivity material in the upper millimeter compared to the centimeter of the diurnal skin depth.

3 Interpretation

The different sensors reacted in distinct ways to the transits. The clearest signal is from the Phobos transit on Sol 501, which lasted 27 seconds. In the following we discuss the signals from this transit in the 135s long window of fig. 1 and table 1.

- barometric pressure and atmospheric temperature: no reaction
- solar array current: Gaussian-like reduction for the duration of transit.
- magnetometers: two components (B_x, B_z) showed a Gaussian-like decrease very similar to the solar array current while B_y showed no reaction. No delay in time between reaction of magnetometers relative to array current.
- surface temperature: initial response as fast as for array current and magnetometer followed by a recovery phase of 1.5 minutes.
- broad-band (VBB) seismometer: clear reaction of U,V and W components. After transformation into canonical Z,N,E-components and removal of the instrument response we get a purely horizontal acceleration (see table 1 and figure in electronic supplement) into NNE direction which is delayed relative to the magnetometer, and array currents by 5 seconds. A recovery phase of 1 minute follows.
- short period (SP) seismometer (see figure in electronic supplement): reaction is compatible with VBB but with lower signal-to-noise ratio.

How can we understand these different reactions? The array current is the most straight forward to interpret: during the transit the solar disc is partially covered by Phobos and hence less radiation reaches the solar arrays. This signal is probably the most direct evidence for the transit considering that the zoom level of the InSight cameras does not allow picture of the sun with high enough resolution (Maki et al., 2018).

The magnetic field variations align perfectly with a scaled version of the array currents. The two wave forms are so similar that a delay of 1 s would be detectable. As pointed out above, this lack of a delay is a strong indication for a cross-talk from the solar array currents leading to an electronically induced magnetic signal.

The Radiometer provides a direct observation of the cooling of the Martian surface during the transit. The cooling amounts to $\Delta T = 2.5K$ for the events on Sols 97 and 501. The skin depth for such a short, 30 s negative heat pulse is only 0.5 - 1.0 mm.

The response of SEIS to the Phobos transit consists of an apparent horizontal acceleration which is delayed relative to the current output of the solar arrays by 5 seconds. (table 1). We have considered several hypothesis to explain this reaction of SEIS to the transits that we will list and discuss in the following:

(A) gravity and pressure signal from atmospheric cooling
(B) contraction of the tether
(C) magnetic sensitivity of VBB leaf springs
(D) thermal leak by convection through contact zone between WTS and soil with subsequent contraction of LVL legs.
(E) thermal conduction through WTS and RWEB
(F) tidally triggered seismicity
(G) thermoelastic response of subsurface

(A) A change in atmospheric temperature across the entire air column above the lander would lead to a change in density and subsequently in a change in pressure. This hypothesis can be discarded because on the one hand the barometer did not show any response and on the other, the reaction of the seismometer would show primarily on the vertical seismometer component: the Newtonian upward acceleration exerted by the high density air masses above the InSight lander (Zürn & Widmer-Schnidrig, 1995).

(B) a contraction of the tether would lead to a force pulling at the load shunt assembly (LSA) toward the lander. SEIS would then tilt towards the lander, opposite to the observation. We thus reject this hypothesis.

(C) The magnetic sensitivity of the VBB leaf springs is on the order of 0.5 nT/(nms^{-2}) (Lognonné et al., 2019). Even when assuming that the same B-field perturbations occurred at the locations of both the magnetometer and SEIS, which is unrealistic, if they are caused by the solar-array current, the magnetic field perturbations (Table 1) of 3 nT would only create a VBB signal of 6 nm/s^2, which is an order of magnitude too small (see table 1). Furthermore we would expect a perfect match of the wave forms (Forbriger (2007)) which is not what we observe. So there are multiple reasons to discard this hypothesis.

(D) The time constants involved are too large: hours rather than seconds (Mimoun, 2017). Note also that each of the LVL legs is thermally protected by its own bellows (Lognonné et al., 2019).

(E) Same as for (D)

(F) The observed signal does not have any similarity with observed marsquakes, especially no highly scattered coda (Giardini et al., 2020). Again, this hypothesis can be excluded.

(G) The hypothesis of a thermoelastic response of the ground and subsequent tilting of the seismometer derives from a fortuitous observation that was made at BFO in 1997 (Zürn & Otto (2000)): when leaving the seismometer vault the technician forgot to switch off the light and later on noticed that the noise level of the long-period data was elevated since the last visit to the vault. This triggered a long series of experiments with artificial heat sources (light bulbs and soldering irons) in the BFO seismometer vault that established that well shielded horizontal long-period seismometers react almost instantaneously to heat input to the seismic pillar. Thermoelastic strains were the only plausible physical mechanism by which these experiments could be explained.

We interpret the observed apparent horizontal acceleration towards NNE as the seismometer response to a tilt down in the SSW direction. The tilt response of the seismometer to Phobos and Deimos transits is shown in table 1. Only the three transits with the highest solar elevation generated a measurable response in the seismometer. Although the azimuth of the sun varied between 126-243°, and the direction towards the main shadow by 7 degree the azimuth of the tilt only varied between 200-211°.

274 A simple model for the tilt consists of areas of shadow under the lander and the WTS that do not
275 change temperature, while the surface everywhere else cools by a few degrees C. This causes a thin
276 layer to thermoelastically contract outside the shadow areas, where RAD is measuring the change in
277 surface temperature (Figure 2). The penetration depth for this temperature perturbation is 0.5-1.0
278 mm. This contracting surface layer is elastically coupled to the material below it, causing thermoelastic
279 stress, strain, tilt and displacement fields in the top few meters, to which the seismometers respond.

3.1 Analog experiment at BFO

281 Since the Phobos transit is a rapid event it is not easy to find a terrestrial analog: on Earth, solar
282 transits take about 3 hours, such that the response is well outside the pass-band of seismometers.
283 Therefore we have chosen to simulate the Phobos transit with an experiment in a well controlled
284 environment of a quiet seismic vault at the Black Forest Observatory (BFO) near Schiltach, Germany.
285 The question we try to answer is if shining a light on a well shielded seismometer can lead to a response
286 at time scales of only a few seconds. Thus we repeat the experiment of Zürn & Otto (2000) but with
287 improved timing accuracy of the switching of the light source. We observe the differential signal of two
288 very broadband seismometers, one shielded with a 1.2 m wide styrofoam cube, but in line of sight of
289 the bulb, the other one installed in a separate vault 100m away in a (dark) post-hole. The difference of
290 the signals of the two sensors is free of noise from marine microseism and semidiurnal tides. Separate
291 power circuits were used for instruments and light, and the experiment was done hours after human
292 operators had left the cavern. The details of the experiment are described in the supplementary
293 material. We find that the signal following the switching of the light bulb are fundamentally equal
294 to the Phobos transit response of SEIS on Mars: 1. No signal is recorded on the vertical component,
295 consistent with tilt. 2. The signal on the horizontal channels has a delay to the input of 12 seconds,
296 compared to the 5 seconds on Mars. 3. A thermal conduction effect is observed only with a time
297 constant of 3 hours, i.e. much longer than the duration of the transit on Mars.

3.2 FE modeling

299 We use a finite element model (FEM) to better understand the amplitude elastic response to the
300 thermally induced stresses at the surface due to the cooling in the regions that suddenly see a drop
301 in solar irradiation. In the shadows of the WTS and the lander with its solar panels and at depth
302 the temperature remains constant. We assume an exponential temperature profile with skin depth
303 of 2mm, a temperature change at the surface of 2 K, a thermal expansion coefficient of 10^{-5}/K, a
304 Poisson ratio of 0.25 and use a domain of $(40\text{m})^3$. The horizontal and vertical resolution in the region
305 of interest are 35 mm and 0.8 mm respectively and element sizes increase with distance. The top
306 surface of the domain is stress free, the bottom boundary is fixed and the four lateral boundaries
307 allow motion only in parallel to the boundary. The isotropic thermal stresses are computed from the
308 assumed thermal profile and then used as the right hand side in the elastostatic equation, which is
309 solved using the finite element method (Schaa et al., 2016).

310 The results in fig. 3 a) and b) demonstrate that the most relevant vertical displacement follows a
311 surprisingly simple pattern with uplift in the shadow and suppression in the previously sun exposed
312 areas and a steep transition between the two regimes within a few centimeters. While the horizontal
313 displacements reach further out, we would not be able to observe them. The tilts associated with the
314 vertical displacement pattern are shown in fig. 3 c): they are concentrated at the shadow boundaries
315 and quickly decay to very small values, including at the location of the SEIS feet. The relative vertical
316 motion of the SEIS feet in this model is at least one order of magnitude smaller than the observation.
317 On the other hand, the strains as shown in fig. 3 d) are nonzero below SEIS and in fact an order of
318 magnitude larger in absolute value than the observed tilt (measured in radians). As a consequence,
319 any heterogeneity or surface topography that causes even small coupling between strains and tilts (e.g.
320 Harrison, 1976; van Driel et al., 2012) is more likely to cause the observed tilts than the prediction
321 from a homogeneous half space model. These strain coupled tilts can take any direction, but as the
322 effect is linear, the direction should be similar for similar shadowing.

3.3 Timing of the transit

324 From the transits signature on the various instruments, it is possible to compare the timing of
325 the Phobos transits with their expected timing from ephemerides models used for the orbit of Phobos.

Relative to mar097 (R. Jacobson & Lainey, 2014), the measured timing of maximal depth in the light curve, as determined from the solar array current, is 8 s early for the Sol 495 transit, 5 s late for the Sol 498 transit, 0.5 s late for the Sol 499 transit and 0.5 s early for the Sol 501 transit, with fit uncertainties of at best ± 0.5 s. As the errors over 1 sec are associated with the low-Sun events in which insolation was dominated by diffuse light, it seems unlikely that they imply errors in the ephemerides. Rather, scattered light responds to the shadow in the dusty atmosphere early as Phobos sets in front of the rising Sun, and late for the reverse. Therefore, the errors in the timing of the maximal depth in the light curves are likely to be due to some atmospheric effects such as dust scattering. Besides, all modeled light curve transits can be fitted with the observations without changing their duration with an accuracy better than 1 s (for a time sampling of one data point every 4 s). This seems to indicate that the mar097 ephemerides are correct in their predictions. Since the accuracy of the Phobos ephemerides should be better than several hundred meters (Jacobson, 2010; R. Jacobson & Lainey, 2014), this would translate into a timing error of less than 0.5 s given Phobos' orbital speed. Further work is needed to study the relation between the observed offsets and the observed depths together with the local time and the Sun's position to model these atmospheric effects and constrain the dust in the Martian atmosphere during the Phobos transits for a given set of Phobos ephemerides. Since the SEIS sensors are by far the ones with the highest sampling rate to ever have observed an transit on Mars (20 sps for the VBB seismometer and 100 sps for SP), we tried to use the signals of different transits as matched filters to estimate the time difference between two following transits (Fig. 2). The timing difference between VBB and RAD or MAG is always larger than the difference between the latter two. This is to be expected, since the effect on VBB is delayed by the thermal conduction of the cooling in the near surface.

4 Discussion

Of all signals, the Solar array currents are the easiest to explain, followed by the surface temperature, as detected by the radiometer. Given that the magnetic field signal matches the timing of the solar array current and that both are absent for near-miss transits, we conclude that the IFG signals are most likely generated by changes in the solar array currents. They can therefore serve to measure the timing of transits, where SAC was only recorded every 30 seconds.

The observed VBB accelerations are compatible with a tilt of SEIS. Futhermore the onset of VBB signal is delayed in time by approx. 5 s relative the the array currents, the radiometer or the magnetometer. Both of these observations match what was observed in the experiment in the BFO seismometer vault: broad-bad seismometers that are very well isolated from heat conduction and from direct solar radiation can still respond within seconds to external irradiation: an observation that we can only explain with a thermoelastic response of the ground and associated tilting of the seismometer. What then is responsible for the thermoelastic deformation? Is it the thermal contrast created by the shadow of the WTS or the lander and its solar arrays? What argues in favor of the lander shadow hypothesis is that it is larger than the WTS shadow and that the tilt azimuths point away from the lander. However the FE modeling for a homogeneous half space predicts that the tilt generated by the lander shadow is too small to explain the observed tilt. A more likely scenario based on the predictions of the FE calculations is that the WTS shadow is responsible for the observed tilt. However, even under the WTS, the tilts predicted by the FE modeling are not what SEIS sensed but instead we propose that strain coupled tilts due to very local heterogeneities generated the observed tilts. This is because the strains under the WTS are more than an order of magnitude larger than the predicted tilts.

5 Summary

We report the observation of eight solar transits by the sensors on the InSight lander. We use these well defined events to better understand the martian environment and how it responds to rapid changes in solar irradiation. The solar array currents have responded to all transits. They are the most sensitive detectors for such events. A drop in ground temperature has been detected for the larger transits while no change in air temperature or barometric pressure was detected. The magnetometer most likely responded to the drop in array currents.

The VBB signals are the most complex ones to explain: strain coupled tilts from thermoelastic strains in the duricrust generated by the shadow of the WTS. The results will help to further constrain the timing of Phobos transits, but also highlight the importance of strain-tilt coupling when modelling seismic responses.
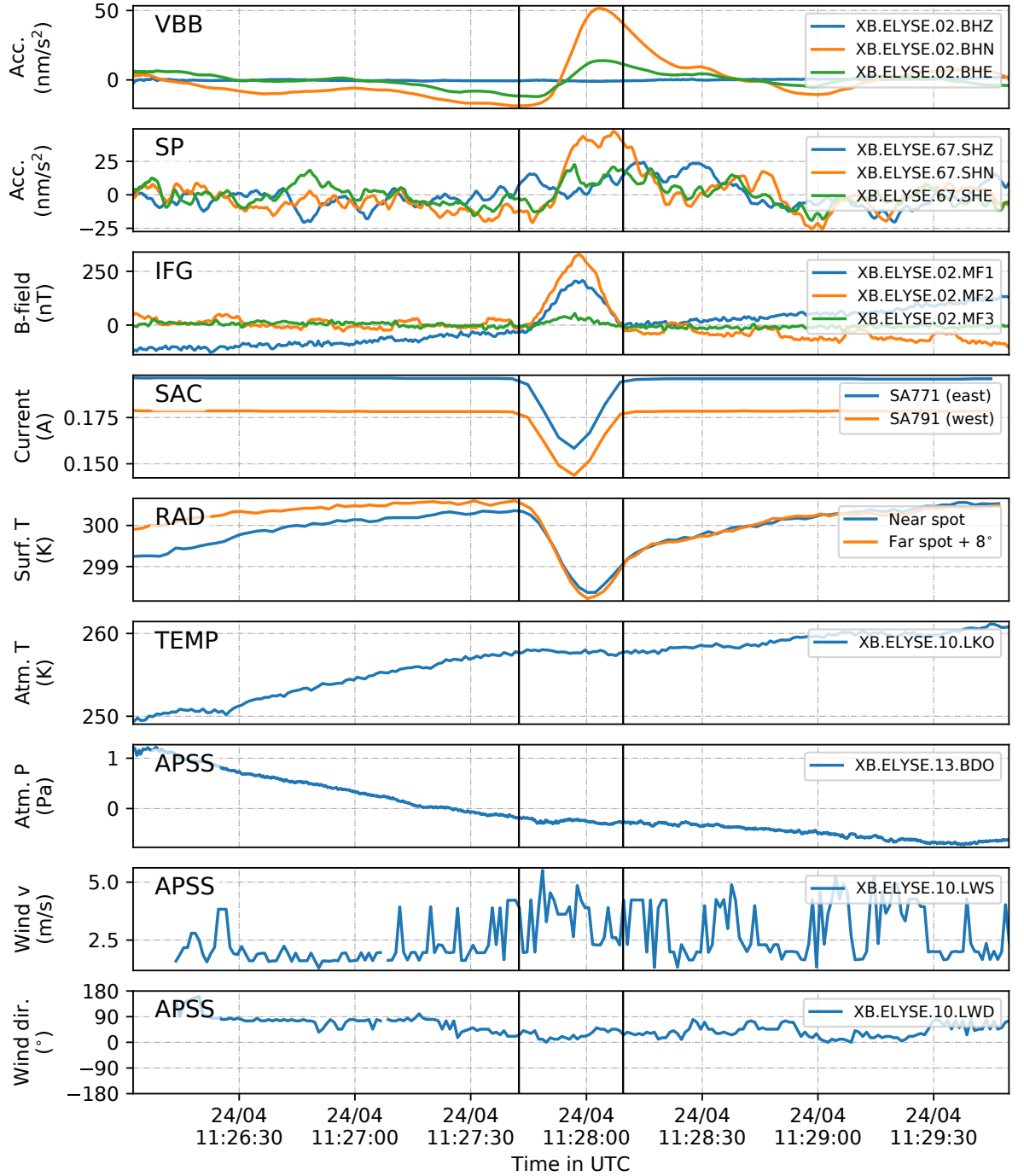
References

Banfield, D., Rodriguez-Manfredi, J. A., Russell, C. T., Rowe, K. M., Leneman, D., Lai, H. R., . . . Banerdt, W. B. (2018, Dec 17). Insight auxiliary payload sensor suite (apss). *Space Science Reviews*, *215*(1), 4. Retrieved from `https://doi.org/10.1007/s11214-018-0570-x` doi: 10.1007/s11214-018-0570-x

Banfield, D., Spiga, A., Newman, C., Forget, F., Lemmon, M., Lorenz, R., . . . Banerdt, W. B. (2020, February). The atmosphere of Mars as observed by InSight. *Nature Geoscience*. doi: 10.1038/s41561-020-0534-0

Bell, J. F., Lemmon, M. T., Duxbury, T. C., Hubbard, M. Y., Wolff, M. J., Squyres, S. W., . . . Ludwinski, J. M. (2005). Solar eclipses of Phobos and Deimos observed from the surface of Mars. *Nature*, *436*(7047), 55–57. doi: 10.1038/nature03437

Betts, B. H., Murray, B. C., & Svitek, T. (1995, March). Thermal inertias in the upper millimeters of the Martian surface derived using Phobos' shadow. *Journal of Geophysical Research*, *100*(E3), 5285-5296. doi: 10.1029/95JE00226

Bills, B. G., Neumann, G. A., Smith, D. E., & Zuber, M. T. (2005). Improved estimate of tidal dissipation within Mars from MOLA observations of the shadow of Phobos. *J. Geophys. Res. E Planets*, *110*(7), 1–15. doi: 10.1029/2004JE002376

Folkner, W. M., Dehant, V., Le Maistre, S., Yseboodt, M., Rivoldini, A., Van Hoolst, T., . . . Golombek, M. P. (2018, August). The Rotation and Interior Structure Experiment on the InSight Mission to Mars. *Space Science Reviews*, *214*(5). doi: 10.1007/s11214-018-0530-5

Forbriger, T. (2007). Reducing magnetic field induced noise in broad-band seismic recordings. *Geophys. J. Int.*, *169*, 240–258.

Garcia, R. F., Kenda, B., Kawamura, T., Spiga, A., Murdoch, N., Lognonné, P. H., . . . Banerdt, W. B. (2020). Pressure Effects on the SEIS-InSight Instrument, Improvement of Seismic Records, and Characterization of Long Period Atmospheric Waves From Ground Displacements. *Journal of Geophysical Research: Planets*, e2019JE006278. doi: 10.1029/2019JE006278

Giardini, D., Lognonné, P., Banerdt, W. B., Pike, W. T., Christensen, U., Ceylan, S., . . . Yana, C. (2020, February). The seismicity of Mars. *Nature Geoscience*. doi: 10.1038/s41561-020-0539-8

Golombek, M., Warner, N. H., Grant, J. A., Hauber, E., Ansan, V., Weitz, C. M., . . . Banerdt, W. B. (2020, December). Geology of the InSight landing site on Mars. *Nature Communications*, *11*(1), 1014. doi: 10.1038/s41467-020-14679-1

Golombek, M., Williams, N., Warner, N. H., Parker, T., Williams, M. G., Daubar, I., . . . Torres, J. (n.d.). Location and Setting of the InSight Lander, Instruments and Landing Site. *Earth Sp. Sci.*(v), 1–68.

Grier, J. A., & Rivkin, A. S. (2019). Chapter 2 - common characteristics of airless bodies. In J. A. Grier & A. S. Rivkin (Eds.), *Airless bodies of the inner solar system* (p. 9 - 26). Elsevier. Retrieved from `http://www.sciencedirect.com/science/article/pii/B9780128092798000020` doi: https://doi.org/10.1016/B978-0-12-809279-8.00002-0

Harrison, J. C. (1976). Cavity and topographic effects in tilt and strain measurement. *J. Geophys. Res.*, *81*(2), 319–328. Retrieved from `http://www.agu.org/journals/ABS/1976/JB081i002p00319.shtml`

Huba, J., & Drob, D. (2017). Sami3 prediction of the impact of the 21 august 2017 total solar eclipse on the ionosphere/plasmasphere system. *Geophysical Research Letters*, *44*(12), 5928–5935.

Jacobson. (2010, jan). THE ORBITS AND MASSES OF THE MARTIAN SATELLITES AND THE LIBRATION OF PHOBOS. *The Astronomical Journal*, *139*(2), 668–679. doi: 10.1088/0004-6256/139/2/668

Jacobson, R., & Lainey, V. (2014, November). Martian satellite orbits and ephemerides. *Planetary and Space Science*, *102*, 35–44. doi: 10.1016/j.pss.2013.06.003

Joy, S. P., Mafi, J. N., & Slavney, S. (2019). Interior Exploration Using Seismic Investigations, Geodesy, and Heat Transport (InSight) Mission Insight Fluxgate Magnetometer (IFG) PDS Archive Software Interface Specification. *urn:nasa:pds:insight-ifg-mars:document:insight-ifg-sis*.

Kenda, B., Drilleau, M., & Lognonne, P. e. a. (2020). Subsurface structure at the insight landing site from compliance measurements by seismic and meteorological experiments. *J. of Geophys. Res. Planets*, *accepted*.

Khan, A., Liebske, C., Rozel, A., Rivoldini, A., Nimmo, F., Connolly, J. A. D., . . . Giardini, D. (2018, feb). A Geophysical Perspective on the Bulk Composition of Mars. *J. Geophys. Res. Planets*,

123(2), 1–37. Retrieved from `http://doi.wiley.com/10.1002/2017JE005371` doi: 10.1002/ 2017JE005371

Kim, J.-H., & Chang, H.-Y. (2018). Statistical analysis of geomagnetic field variations during solar eclipses. *Advances in Space Research*, 61(8), 2040 - 2049. Retrieved from `http://www.sciencedirect.com/science/article/pii/S0273117718300656` doi: https://doi.org/10.1016/ j.asr.2018.01.022

Ledger, E. (1879). The eclipses of the satellites of Mars. *Obs.*, 3, 191–193.

Lognonné, P., Banerdt, W. B., Giardini, D., Pike, W. T., Christensen, U., Laudet, P., ... Wookey, J. (2019, January). SEIS: Insight's Seismic Experiment for Internal Structure of Mars. *Space Science Reviews*, 215(1). doi: 10.1007/s11214-018-0574-6

Lognonné, P., SEISteam, & Widmer-Schnidrig, R. (2019). Seis: Insight's seismic experiment for internal structure of mars. *Space Sci Rev*, 215(12). doi: 10.1007/s11214-018-0574-6

Lorenz, R. D., Lemmon, M. T., Maki, J., Banfield, D., Spiga, A., Charalambous, C., ... Banerdt, W. B. (2020). Scientific observations with the InSight solar arrays: Dust, clouds and eclipses on mars. *Earth and Space Science*.

Lorenz, R. D., Lemmon, M. T., & Mueller, N. (2020). A transit lightcurve of Deimos, observed with the insight solar arrays. *Research Notes of the American Astronomical Society*, 4. Retrieved from `https://doi.org/10.3847/2515-5172/ab8d21`

Maki, J. N., Golombek, M., Deen, R., Abarca, H., Sorice, C., Goodsall, T., ... Banerdt, W. B. (2018, September). The Color Cameras on the InSight Lander. *Space Science Reviews*, 214(6). doi: 10.1007/s11214-018-0536-z

Mimoun, M. N. L. P. e. a., David. (2017). The noise model of the seis seismometer of the insight mission to mars. *Space Sci Rev*, 211, 383-428. doi: https://doi.org/10.1007/s11214-017-0409-x

Mueller, N., Knollenberg, J., Grott, M., Kopp, E., Walter, I., Krause, C., ... Smrekar, S. (2020). Calibration of the HP^3 radiometer on InSight. *Earth and Space Science*. doi: 10.1029/2020EA001086

Mueller, N. T., Knollenberg, J., Grott, M., Kopp, E., Walter, I., Krause, C., ... Smrekar, S. (2020). Calibration of the hp3 radiometer on insight. *Earth and Space Science*, 7(5), e2020EA001086. Retrieved from `https://agupubs.onlinelibrary.wiley.com/doi/abs/10.1029/2020EA001086` (e2020EA001086 10.1029/2020EA001086) doi: 10.1029/2020EA001086

Murdoch, N., Spiga, A., Lorenz, R., Garcia, R., Perrin, C., Widmer-Schnidrig, R., ... Banerdt, W. (under review in this issue). Constraining Martian regolith parameters and vortex trajectories from combined seismic and meteorological measurements. *Journal of Geophysical Research: Planets*.

Nimmo, F., & Faul, U. H. (2013). Dissipation at tidal and seismic frequencies in a melt-free, anhydrous Mars. *J. Geophys. Res. E Planets*, 118(12), 2558–2569. doi: 10.1002/2013JE004499

Reinisch, B., Dandenault, P., Galkin, I., Hamel, R., & Richards, P. (2018). Investigation of the electron density variation during the 21 august 2017 solar eclipse. *Geophysical Research Letters*, 45(3), 1253–1261.

Schaa, R., Gross, L., & Du Plessis, J. (2016). PDE-based geophysical modelling using finite elements: Examples from 3D resistivity and 2D magnetotellurics. *J. Geophys. Eng.*, 13(2), S59–S73. Retrieved from `http://dx.doi.org/10.1088/1742-2132/13/2/S59` doi: 10.1088/1742-2132/13/2/S59

Schweitzer, J., Pirli, M., Roth, M., & Kvaerna, T. (2014, jul). TROLL: A New, Very Broadband Seismic Station in Antarctica. *Seismol. Res. Lett.*, 85(4), 852–862. Retrieved from `https://pubs.geoscienceworld.org/srl/article/85/4/852-862/315410` doi: 10.1785/0220130223

Spiga, A., Banfield, D., Teanby, N. A., Forget, F., Lucas, A., Kenda, B., ... Banerdt, W. B. (2018, October). Atmospheric Science with InSight. *Space Science Reviews*, 214(7). doi: 10.1007/s11214-018-0543-0

Spohn, T., Grott, M., Smrekar, S. E., Knollenberg, J., Hudson, T. L., Krause, C., ... Banerdt, W. B. (2018, August). The Heat Flow and Physical Properties Package (HP3) for the InSight Mission. *Space Science Reviews*, 214(5). doi: 10.1007/s11214-018-0531-4

Usui, T., Kuramoto, K., & Kawakatsu, Y. (2018). Martian moons exploration (mmx): Japanese phobos sample return mission. In *42nd cospar scientific assembly* (Vol. 42).

van Driel, M., Wassermann, J., Nader, M.-F., Schuberth, B. S. A., & Igel, H. (2012, mar). Strain rotation coupling and its implications on the measurement of rotational ground motions. *J. Seismol.*, 16, 657–668. Retrieved from `http://www.springerlink.com/index/10.1007/s10950-012-9296-5` doi: 10.1007/s10950-012-9296-5

Zürn, W., & Otto, H. (2000). Lights or heat in the seismic vault, Black Forest Observatory (BFO). *Internal Technical Report*, 3.

511   Zürn, W., & Widmer-Schnidrig, R. (1995). On noise reduction in vertical seismic records below 2 mHz
512   using local barometric pressure. *Geophys. Res. Lett.*, *22*(24), 3537–3540. doi: 10.1029/95GL03369
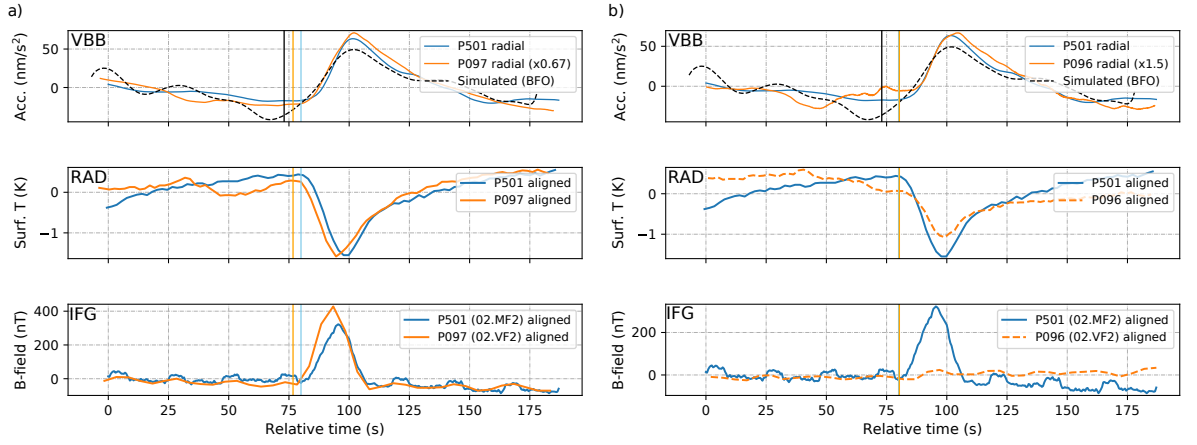
Figure 1. Data recorded during the Phobos transit at the InSight location on Sol 501. Channels are from top: band-pass filtered acceleration data (first order Butterworth, 0.005–0.2 Hz) for the VBB and SP seismometers, demeaned magnetic data (IFG: InSight Fluxgate Magnometer), solar array currents (SAC), radiometer (RAD) surface temperatures of the near and far spot (see N. T. Mueller et al., 2020), as well as atmospheric temperature, atmospheric pressure, wind speed and wind direction (pos. from North) as part of the Auxiliary Payload Sensor Suite (APSS, Banfield et al., 2018). Black vertical lines: eclipse start and end times according to the JPL ephemeris mar097 (R. Jacobson & Lainey, 2014). Note that atmospheric temperature and pressure as well as the wind show no significant changes during the eclipse. For the details of the channel naming see Lognonné et al. (2019).
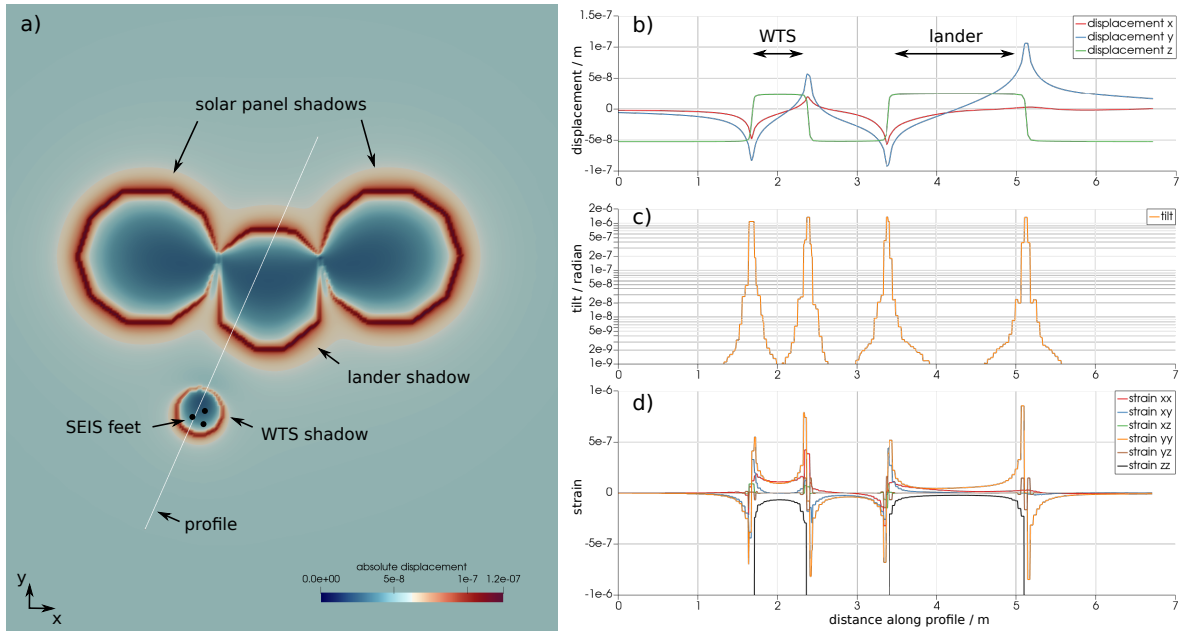
Table 1. Eclipses by the martian moons Phobos and Deimos at the InSight location (LAT = 4.5024°, LON = 135.6234°) since landing on November 26, 2018 (Sol 0). We distinguish between three different eclipse types: annular = moon appears entirely within the Sun; transit = center of moon appears within the Sun; graze = parts of moon but not its center appear within the Sun. The time of the maximum of an eclipse is defined by the time of the minimum angular separation (MAS) between the Sun and moon. UTC and LTST (local true solar time), Sun azimuth (Azi), and moon elevation (Ele), are all with respect to the MAS time. Duration (Dur) is between first and last apparent contact. All these measures are based on the JPL ephemeris mar097 (R. Jacobson & Lainey, 2014). For the magnetic field data (IFG: InSight Fluxgate Magnetometer), changes in each component and changes in the magnitude of the total field are listed in the lander level frame (X points north, Y east and Z vertically down). The changes in the solar array current (SAC) channels are given in Ampere and the corresponding % drop from baseline. On sol 99 channel 772 shows an increase and 702 a decrease and thus no average value is calculated.

All VBB and SP seismic data were 0.001–0.1 Hz band-pass filtered prior to our measurements (first order Butterworth).

MOON	ECLIPSE						VBB			SP			IFG				SAC	
	Type MAS (mrad)	UTC of MAS	LTST of MAS	Azi. (°)	Ele. (°)	Dur. (s)	Tilt azi. (°)	Acc. R (nms^{-2})	Tilt (nrad)	Tilt azi. (°)	Acc. R (nms^{-2})	Tilt (nrad)	δB_X (nT)	δB_Y (nT)	δB_Z (nT)	δB_{Total} (nT)	$\delta SAC(771/791)$ (A)	$\delta SAC(772/792)$ (A)
Phobos	Transit -2.61	2020-04-24 11:27:56	501M 12:03:34	186	81	27	200±1	84±7	23±2	201±7	76±10	20±3	3	0	0.2	-2.1	0.04 (19%)	1 (19%)
Phobos	Transit -3.12	2020-04-22 13:52:39	499M 15:41:28	262	34	28	–	–	–	–	–	–	0	0	0	0	0.005 (10%)	0.1 (10%)
Phobos	Annular 1.73	2020-04-21 14:58:53	498M 17:24:27	266	9	36	–	–	–	–	–	–	0	0	0	0	0.0008 (10%)	0.02 (13%)
Phobos	Graze -4.65	2020-04-21 06:35:44	498M 09:14:46	100	48	12	–	–	–	–	–	–	0	0	0	0	no data	no data
Phobos	Transit -2.97	2020-04-18 01:52:20	495M 06:34:29	93	8	30	–	–	–	–	–	–	0	0	0	0	0.0002 (2%)	channels inconsistent
Phobos	Graze -3.49	2019-03-08 15:37:31	099M 15:53:18	263	31	23	–	–	–	–	–	–	0	0	0	0	0.002 (3%)	channels inconsistent
Phobos	Transit 2.16	2019-03-06 09:34:08	097M 11:16:10	126	76	28	211±2	156±16	42±4	206±5	124±13	33±4	2	4	3.3	-0.6	0.04 (14%)	no data
Phobos	Transit 2.77	2019-03-05 10:48:17	096M 13:06:39	243	71	26	205±8	61±9	16±2	196±13	68±10	18±3	1	0	2.7	-1.9	0.03 (12%)	no data
Deimos	Graze -3.18	2020-04-05 04:38:57	482M 17:36:56	270	6	47	–	–	–	–	–	–	0	0	0	0	0 (0%)	0 (0%)
Deimos	Annular -0.03	2020-04-03 21:28:13	481M 11:16:10	107	79	126	–	–	–	–	–	–	0	0	0	0	0.0 (0%)	no data

Figure 2. Seismic, radiometer, and magnetic data during the eclipses; a) Sols 501 and 97, and b) Sols 501 and 96. Top panels: VBB radial acceleration data (same filter as in Tab. 1) cross-correlated to align the events; the orange lines are shifted by -3.3 s in a) and +0.3 s in b) where negative means shift to the left and vice versa. These shift times are with respect to the eclipse start times calculated from the JPL ephemeris mar097 (R. Jacobson & Lainey, 2014). Black line: simulated acceleration for an eclipse-like event derived from our light bulb experiment in the seismometer vault at the Black Forest Observatory (BFO, see electronic supplements). Vertical lines: start times of the respective events. Middle panels: radiometer surface temperatures (RAD, near spot) during the eclipses. RAD data were shifted like the seismic data in the top panels. Bottom panels: Magnetic data (IFG, sensor 2) during the eclipses. Magnetometer data were shifted like the seismic data in the top panels. Note that for illustrational purposes the second seismic event was scaled in amplitude, and surface temperature and magnetic field data were demeaned.

Figure 3. Finite element simulation of thermoelastic deformation in a medium with homogeneous elastic parameters for the shadows of P501. a) Absolute value of the displacement, location of the SEIS feet and indication of the profile used in b)–d). b) 3-component displacements, c) tilt, and d) strains observed along the profile.